JOURNAL OF THERMOPHYSICS AND HEAT TRANSFER
Vol. 12, No. 4, October–December 1998

# Statistical Simulation of Nonequilibrium Rarefied Flows with Quasiclassical Vibrational Energy Transfer Models

S. F. Gimelshein,* M. S. Ivanov,† G. N. Markelov‡
*Institute of Theoretical and Applied Mechanics, 630090 Novosibirsk, Russia*
and
Yu. E. Gorbachev§
*Institute for High-Performance Computing and Data Bases, 194291 St. Petersburg, Russia*

**A new model for vibration–vibration–translation energy exchange is presented that is suitable for the direct simulation Monte-Carlo (DSMC) method. The model is based on a quasiclassical description of vibrationally inelastic collision processes and on the mean frequency approximation. The model has been incorporated into the DSMC majorant frequency scheme and used in computations. The model is used for the flow about a hyperboloid with a flare, and the influence of vibration–vibration energy transfer and variable molecular diameters is examined. The comparison with available experimental data has been performed for the near-continuum dissociating nitrogen flow about a wedge.**

## Introduction

PRACTICAL demands associated with the hypersonic flight of modern space vehicles currently stimulate an increasing interest in the problems of hypersonic rarefied aerothermodynamics. A rarefied flow regime conventionally covers high altitudes of flight, from orbital down to about 80 km, where rarefied hypersonic flow transitions to hypersonic continuum. Furthermore, local rarefied flows occur near space vehicles' sharp leading edges at significantly reduced altitudes, and under conditions where the vehicle as a whole is in the continuum regime.

The physical and chemical effects that take place at hypersonic speeds are mainly related to a rapid increase of the temperature behind the shock wave at high Mach numbers. The temperature reaches these high values when the excitation of molecular vibrations occurs, followed by chemical reactions such as dissociation, exchange, and recombination, if the pressure is high enough. For very high temperatures, ionization and radiation are also observed. For high altitudes, the thermal and chemical relaxation lengths are comparable with or larger than the correspondent flow scale, and the difference in temperatures of translational, rotational, and vibrational molecular modes becomes determining. Moreover, in some cases, the introduction of temperatures themselves for the internal degrees of freedom became senseless. An accurate description of hypersonic low-density aerodynamics requires that the kinetic approach be used.

The direct simulation Monte Carlo (DSMC) method has become the main tool of rarefied hypersonic aerothermodynamics for studying complex multidimensional flows. This is primarily conditioned by a number of its obvious merits: the comparative simplicity of transition from one-dimensional problems to two- and three-dimensional ones, and a possibility of using various models of particle interaction, including the models of internal degrees of freedom and chemical reactions, without substantial complication of the computational algorithm. This last feature is of primary importance for modeling high-temperature flows with real gas effects.

In continuum gasdynamics the real gas effects are usually understood as high-temperature phenomena characterized by molecular vibration, dissociation, ionization, surface chemical reaction, and radiation. In describing the problems of rarefied gasdynamics in which a large shock-wave thickness and rarefaction effects exert the determining influence on the flow structure, it is convenient to consider the real gas effects in a wider sense. As applied to kinetic methods based on the microscopic approach, particularly the DSMC method, it seems natural to relate the real gas effects with all phenomena associated with molecular collisions: (P1) elastic collisions, (P2) rotational excitation, (P3) vibrational excitation, (P4) bulk chemical reactions, (P5) ionization, (P6) radiation, and (P7) gas-surface interaction.

In the altitude range of 80–90 km, the flow about space vehicles that re-enter at a speed of 8 km/s is near-continuum, and an adequate description of thermochemical nonequilibrium associated with processes P2 and, particularly, P3 and P4 (vibrational and chemical relaxation lengths become comparable with the vehicle size) is indispensable. The specific features of these processes, such as a large number of open channels and wide intervals of energy, quantum numbers, and interaction parameters, require an appropriate choice of research methods to be used. One of the most effective approaches is the quasiclassical approximation of the scattering theory.

The main objective of the work is to present DSMC models for the P3 process based on a quasiclassical approximation of the scattering theory. The results of the approach based on a new variant of the quasiclassical multidimensional scattering theory for the description of the vibration–rotation–translation exchange of polyatomic molecules[1] are used here. The anharmonicity effects are included, and the multiquantum transition probabilities are obtained automatically without a compilation of different approximations.

The principal advantage of the quasiclassical approach is its ability to consider all collisional aspects from one point of view. Although the main attention here is paid to the processes

Presented as Paper 97-2585 at the AIAA 32nd Thermophysics Conference, Atlanta, GA, June 23–25, 1997; received July 14, 1997; revision received March 2, 1998; accepted for publication May 4, 1998. 

*Research Scientist, Computational Aerodynamics Laboratory; currently at Cornell University, Ithaca, NY 14853-7501. E-mail: sergey@mae.cornell.edu.

†Head, Computational Aerodynamics Laboratory. E-mail: ivanov@itam.nsc.ru. Member AIAA.

‡Research Scientist, Computational Aerodynamics Laboratory. E-mail: markelov@itam.nsc.ru.

§Deputy director. E-mail: gorbachev@hm.csa.ru.

of vibrational energy exchange, an application of this approach in the framework of the DSMC method for modeling rotation–translation energy transfer and chemical reactions is being planned. This paper is a continuation of our previous work,[2] where a new model for vibration–translation (VT) energy transfer was proposed and its influence on the high-temperature reactive flows was studied. The refinement of this model is presented later in this paper, which implies the consideration of vibration–vibration (VV) energy transfer, and incorporates variable diameters of molecules, depending on their rotational and vibrational states. This paper presents the first attempt to assess the influence of VV transitions and variable molecular diameters on a rarefied hypersonic flow. An important topic is also the examination of the P3 model impact on chemically reactive flows. All computations were conducted with the DSMC code SMILE, developed at ITAM, Novosibirsk.

## Numerical Method

The DSMC method may be constructed directly from the spatially nonuniform Leontovich master kinetic equation for the $N$-particle distribution function.[3] The direct use of the $N$-particle master equation is quite natural here because in DSMC calculations a finite system of simulation molecules is always considered. Because the Boltzmann equation may be derived from the master kinetic equation for an $N$-particle system under the condition of molecular chaos, the DSMC method is regarded in a certain sense as a numerical method for solving the Boltzmann equation.

Depending on the kind of regularization of the master kinetic equation, two different majorant frequency schemes, cell and free cell, were derived by Ivanov and Rogasinsky.[3] In SMILE, the method is applied that combines both of these schemes.[4] The computational domain is divided into uniform "background cells." The majorant frequency of collisions for each background cell is

$$\nu_l^m = \frac{N_l(N_l - 1)}{2} [\sigma(g)g]_{\max} \frac{1}{\varepsilon_l}$$

where $N_l$ is the number of molecules in a cell, and $\varepsilon_l$ is the volume of the interaction region in the $l$th cell. The linear size of this interaction region governs the local collision resolution. The adaptation of this linear size to local gradients and local mean free paths occurs during the modeling process. In an undisturbed flow, the volume of the interaction region coincides with the volume of background cells, and this volume is considerably reduced in the shock fronts where the flow is highly nonequilibrium. Thus, the cell scheme is applied far from the body, and to provide for a high spatial resolution, the free-cell scheme is used in each background cell (similar to a zoom lens) in the zone of strong gradients. Note that the indexing of molecules by cells is carried out only for the background uniform Cartesian mesh. Such a combined usage of cell and free cell schemes made it possible to achieve an adequate spatial resolution in the entire flowfield. In conjunction with the absence of any restrictions on the number of particles in each cell, this allows one to simulate the flow at very small Knudsen numbers.

## Collision Models

The DSMC models for processes P1–P4 used in the computations are specified in this section. The main attention is paid to new models of VT and VV energy exchange.

The variable soft sphere model has been used for intermolecular potential.[5] Parameters of the model (viscosity-temperature dependence and constant in the scattering law) were taken from Ref. 6. To model the rotation–translation energy exchange, the Larsen–Borgnakke (LB) model with discrete energy levels has been used, coupled with the particle selection procedure.[7,8] The temperature-dependent rotational relaxation number, $Z_r$, was employed, with the dependence taken from Ref. 9. The model of chemical reactions was utilized to simulate dissociation reactions.[2] In this model, vibration-dissociation coupling is included by using specific chemical reaction rate constants for each vibrational level.

### VT Energy Transfer

A quasiclassical theory developed by Bogdanov et al.[1] gives accurate but complicated expressions (shown previously as multidimensional quadrature representations) for inelastic cross sections. At the same time this approach is rather rich for building further approximations. One of them, namely, a mean frequency approximation, is proposed in this paper that implies the arithmetic average of initial and final states, both internal and translational energies, to be taken into consideration. This allows one to simplify the expressions for the correspondent transition probabilities derived by the use of generalized eikonal approximation.[1] The approximation used here results in minor changes in formulas as compared with Ref. 2.

Depending on the adiabatic parameter, $\lambda_m$, all collisions are classified into three groups: slow ($\lambda_m > \lambda_2 > 1$), fast ($\lambda_m < \lambda_1 < 1$), and intermediate ($\lambda_1 < \lambda_m < \lambda_2$). The adiabatic parameter is

$$\lambda_m = \omega(n_m)(d/v_m)$$

where

$$\omega(n_m) = [\omega(n_i) + \omega(n_f)]/2$$

$$\omega(n_k) = \omega_e[1 - 2x_e(n_k + 0.5)], \qquad k = i, f$$

$$v_m = \sqrt{2E_m/\mu}, \qquad E_m = (E_i + E_f)/2$$

$n$ is the vibrational quantum number, subscripts $i$ and $f$ refer to the initial and final channels (pre- and postcollision states) respectively, $v_m$ and $E_m$ are the mean velocity and energy of translational motion, $\omega_e$ is the oscillator frequency, $x_e$ is the anharmonicity parameter, $\mu$ is the reduced mass of colliding particles, and $d$ is the parameter of the Morse potential that is used for description of intermolecular interactions

$$V(R) = D\{\exp[-2(R - R_0)/d] - 2\exp[-(R - R_0)/d]\}$$

For slow collisions the VT cross section may be written as

$$\sigma_{n_i \to n_f} = \sigma_T \frac{v_f}{v_i} A_{\mathrm{VT}} \exp\left[-2\Delta_n \lambda_m \arctan\left(\sqrt{\frac{E_m}{D}}\right)\right] \Bigg/ \left\{\Delta_n \lambda_m \left[\arctan\left(\sqrt{\frac{E_m}{D}}\right) - \sqrt{\frac{E_m}{D}} \Bigg/ \left(\frac{E_m}{D} + 1\right)\right]\right\} \tag{1}$$

where

$$A_{\mathrm{VT}} = \frac{\varepsilon_m^{\Delta_n}}{(\Delta_n!)^2} \left\{\frac{\pi d}{2\hbar} [a_1 \mu d \omega(n_m) - (2a_2 - a_1)\sqrt{2\mu D}]\right\}^{2\Delta_n}$$

$\Delta_n = |n_f - n_i|$, $\varepsilon_m = (\varepsilon_i + \varepsilon_f)/2$, $\varepsilon_k = (k + 0.5)[1 - x_e(k + 0.5)]$, $k = i, f$, $a_1$ and $a_2$ are the potential anisotropy parameters; $\sigma_T$ is the total elastic cross section, the expression for which is taken from Ref. 10 for the Lennard–Jones potential as

$$\sigma_T = \pi\sigma_0^2 \left\{2\left(\frac{5\pi\kappa\sigma_0}{4\hbar v_m}\right)^{2/5} + 1 + \frac{1}{6}\left[1 + \ell n\left(\sqrt{5\pi}\frac{4\kappa}{E_m + 4\pi\kappa}\right)\right]\right\}$$

where $\kappa$ and $\sigma_0$ are the parameters of Lennard–Jones potential

$$V(r) = 4\kappa\left[\left(\frac{\sigma_0}{r}\right)^{12} - \left(\frac{\sigma_0}{r}\right)^{6}\right]$$

It should be noted that $\sigma_T$ may be computed using any potential, the choice of which is determined by the convenience, with the only restriction that the potential must correlate with the real interaction. In the case of the Lennard–Jones potential, the parameters $\kappa$ and $\sigma_0$ should be associated with the corresponding parameters of the Morse potential. This requirement is satisfied with

$$\kappa = D, \qquad \sigma_0 = R_0/2^{1/6}$$

The VT cross section for slow collisions thus depends on the translational energies of colliding particles and on the initial and final vibrational levels of the molecule (but not on the vibrational level of its collision partner). This dependence also retains for fast collisions, where the VT cross section is

$$\sigma_{n_i\to n_f} = 2\pi d^2 \frac{v_f}{v_i}\int_{x_0}^{\infty} x\left\{1 - \frac{D}{E_m}e^{-(x-x_{00})} \times [e^{-(x-x_{00})}(1-x) - 2 + x]\right\}\{J_{\Delta_n}[|F(x)|]\}^2\,dx \qquad (2)$$

where $J_\Delta(x)$ is a Bessel function, $x_0 = x_{00} - \ell n(1 + \sqrt{1 + E_m/D})$, $x_{00} = R_0/d$, and

$$F(x) = \frac{Dd}{v_m\hbar}\sqrt{\pi x\varepsilon_m}e^{-(x-x_{00})}[a_1 e^{-(x-x_{00})} - 2\sqrt{2}a_2]$$

In the intermediate region $\lambda_2 > \lambda_m > \lambda_1$, the VT cross section is calculated by interpolation of cross sections for slow and fast collisions

$$\sigma_{n_i\to n_f,\lambda_m} = \exp\left[\frac{\lambda_2 - \lambda_m}{\lambda_2 - \lambda_1}\ell n(\sigma_{n_i\to n_f,\lambda_1}) + \frac{\lambda_m - \lambda_1}{\lambda_2 - \lambda_1}\ell n(\sigma_{n_i\to n_f,\lambda_2})\right] \qquad (3)$$

To strictly satisfy the detailed balance requirement, expressions (1–3) are only used for $n_i < n_f$. The cross sections for $n_i > n_f$ are calculated with

$$\sigma_{n_f\to n_i} = (v_i^2/v_f^2)\sigma_{n_i\to n_f}$$

which enables one to capture the detailed balance.

### VV Energy Transfer

The quasiclassical approach is also applied for VV energy transfer, and the mean frequency approximation is used again.

Adiabatic parameters $\lambda^+$ and $\lambda^-$ are introduced as

$$\lambda^{\pm} = \omega^{\pm}(n_m)d/v_m, \qquad \omega^{\pm}(n_m) = [\omega^{\pm}(n_i) + \omega^{\pm}(n_f)]/2$$
$$\omega^{\pm}(n_i) = |\omega(n_{i1}) \pm \omega(n_{i2})|, \qquad \omega^{\pm}(n_f) = |\omega(n_{f1}) \pm \omega(n_{f2})|$$

Here subscripts 1 and 2 indicate two colliding particles. In the case when $\lambda^+ > 1$, the abiabatic propensity rules determine the process of energy exchange.[1] This means that only generalized isoquantum transitions are allowed

$$\Delta n_1 = -\Delta n_2$$

where $\Delta n_k = n_{fk} - n_{ik}$, $k = 1, 2$. This case for a wide range of collision energies; therefore we use this rule hereinafter.

Depending on the adiabatic parameter $\lambda^-$, the collisions are classified into three groups: slow ($\lambda^- > \lambda_2 > 1$), fast ($\lambda^- < \lambda_1 < 1$) and intermediate ($\lambda_1 < \lambda^- < \lambda_2$). For slow collisions

$$\sigma^{n_{i1}\to n_{f1}}_{n_{i2}\to n_{f2}} = (v_f/v_i)\sigma_0 P_{VV} \qquad (4)$$

where

$$P_{VV} = \frac{A_{VV}\exp\left\{-2\lambda^-\Delta^-\arctan\left(\sqrt{\frac{E_m}{D}}\right)\right\}}{\lambda^-\Delta^-\left[\arctan\left(\sqrt{\frac{E_m}{D}}\right) - \sqrt{\frac{E_m}{D}}\Big/\left(\frac{E_m}{D} + 1\right)\right]}$$

$$\Delta^- = |\Delta n_1 - \Delta n_2|/2$$

$$A_{VV} = \frac{G_{VV}}{\Gamma^2(\Delta^- + 1)}\left\{\frac{\pi d}{2\hbar}[a_1\omega^-(n_m)\mu d - (2a_2 - a_1)(2\mu D)^{1/2}]\right\}^{2\Delta^-}$$

$$G_{VV} = (\varepsilon_{m1}\varepsilon_{m2}/4)^{\Delta^-}$$

The VV cross section is therefore a function of the translational energies and vibrational energies of both collision partners before and after collision. For fast collisions, this dependence takes the form

$$\sigma^{n_{i1}\to n_{f1}}_{n_{i2}\to n_{f2}} = 2\pi d^2\frac{v_f}{v_i}\int_{x_0}^{\infty} x\left\{1 - \frac{D}{E_m}e^{(x-x_{00})} \times [e^{-(x-x_{00})}(1-x) - 2 + x]\right\}\{J_{\Delta^-}[|F(k,x)|]\}^2\,dx \qquad (5)$$

where

$$x_0 = x_{00} - \ell n(1 + \sqrt{1 + E_m/D}), \qquad x_{00} = R_0/d$$
$$F(k,x) = Dd/(2v_m\hbar)\sqrt{\pi x\varepsilon_{m1}\varepsilon_{m2}}e^{-(x-x_{00})}[a_1 e^{-(x-x_{00})} - 2\sqrt{2}a_2]$$

In the intermediate region, an exponential interpolation of Eqs. (4) and (6) is used similar to Eq. (3).

### Variable Molecular Diameters

When vibrational and rotational modes of a molecule are excited, its diameter increases. In the present paper, an expression[11] is used for the mean molecular diameter $\langle d_m\rangle$ of vibrationally and rotationally excited diatomic molecule in the electronic ground state

$$\langle d_m\rangle = \langle R_{v,J}\rangle + 2.25\ (10^{-10}m)$$

where

$$\langle R_{v,J}\rangle = R_e + \beta^{-1}\left(\delta_* + \ell n\frac{1 + \sqrt{1 - \varepsilon_*^2}}{2}\right)$$

$\beta$ and $R_e$ are the parameters of the Morse potential, and $\delta_*$ and $\varepsilon_*$ are the functions of vibrational ($v$) and rotational ($J$) quantum states of the molecule.

The dependence of the molecular diameter on the internal state is significant for molecules with large rotational and vibrational energies. The parameter $(d_{v,J}/d_{0,0} - 1) \times 100$ for oxygen, $O_2$, is given in Fig. 1. It shows an increase of molecular diameter by a factor up to 35% for the upper rotational and vibrational levels.

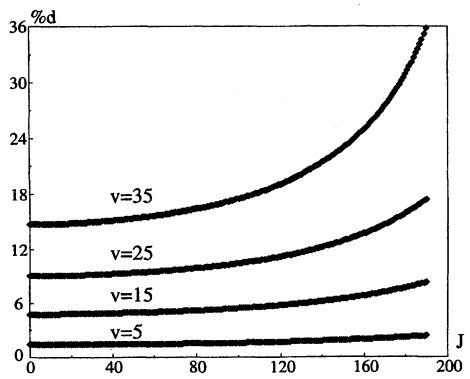


**Fig. 1 Molecular diameter as a function of rotational and vibrational levels.**

## Implementation of VVT Model

In this section, some DSMC code-related issues are discussed connected with the implementation of the new VVT model, and also the values of model parameters are given for nitrogen and oxygen.

The procedure of simulation of collisions consists of a few successive steps. Initially, after checking over relative collision velocities, colliding pairs react (dissociate, in the particular case) with a certain reaction probability. If the reaction did not occur, an elastic or inelastic collision would take place. Such a collision comprises successive checks if there are RT, VT, and VV energy exchanges. For both RT and VT processes, only one molecule can change its rotational and/or vibrational energy in a collision. RT, VT, and VV processes are considered independent (all of those may occur during one collision). In contrast to Ref. 8, where multiple relaxation was prohibited to provide the correct rotational and vibrational relaxation rates, in the present model VT and VV rates are controlled by the corresponding quasiclassical cross sections, and the influence of RT exchange on vibrational processes is negligibly small.

Because expressions (1–5) are rather cumbersome, special arrays for VT and VV transition probabilities are calculated prior to the main computations. These arrays depend only on molecular species of colliding pairs and, therefore, they are computed only once and then stored in the database.

Equations (1–5) specify the cross sections of VT and VV processes. The correspondent probabilities needed in computations are obtained through $P_{(1-5)} = (\sigma_{(1-5)}/\sigma_{T,\mathrm{VSS}})$ to preserve the correct rates of VT and VV processes. The calculation showed that the probabilities of VT or VV transition of molecules on a vibrational level $v$ to some other level do not exceed the unity in the entire temperature range under consideration (up to 25,000 K), despite the fact that the total collision cross section for a Lennard–Jones potential is several times larger than that for a VSS model.

Owing to the use of precalculated probability arrays, the computational efficiency of the new VVT model is sufficiently high. For high temperatures it is comparable with that for LB model (particle selection with constant $Z_v$), and for low temperatures it is even somewhat higher.

Using the majorant frequency algorithm provides an easy and straightforward implementation of variable molecular diameters, and the total efficiency decreases only a few percent.

Two test gases, nitrogen and oxygen, have been taken for computations. The intermolecular potential parameters may be estimated by comparison of the simple potential model, used in our calculations, with a more precise one obtained theoretically or experimentally. These parameters may also be obtained as a result of a comparison of some characteristics calculated on the base of model potential with experimental data. Here we used the mixed approach and chose the potential well depth and interaction radius values from the data on the potential surface. With other parameters, including model parameters $\lambda_{1,2}$, we chose the best agreement of calculated rate constants with measured ones.[12] For the $O_2$–$O_2$ system we use $D = 1.65 \times 10^{-21}J$, $d = 6.09 \times 10^{-11}m$, $R_0 = 3.86 \times 10^{-10}m$, $a_1 = 0.33$, $a_2 = 0$. For the $O_2$–O system all parameters are the same except the anisotropy parameter $a_1 = 0.66$. The $N_2$–$N_2$ system is specified with the potential parameters $D = 1.56 \times 10^{-21}J$, $d = 6.09 \times 10^{-11}m$, $R_0 = 4.07 \times 10^{-10}m$, $a_1 = 0.2$, $a_2 = 0$, and for $O_2$–O $a_1 = 0.6$. For all cases $\lambda_1 = 1.0$, $\lambda_2 = 3.5$ were used. Parameters $a_1$ and $a_2$, and also $\lambda_1$ and $\lambda_2$, are selected[2] so that the rate of VT $1 \rightarrow 0$ transition is in a reasonable agreement with data[13] for low temperatures and data[14] for high temperatures.

## Results and Discussion

### Homogeneous Adiabatic Relaxation

Prior to the two-dimensional and axisymmetric computations, the simulations of a zero-dimensional adiabatic box relaxation have been performed for validation and comparison purposes using different models of vibrational modes. The LB model and the quasiclassical model with VT and VV energy transfer (VVT model) were used here. For the LB model, a constant vibrational relaxation number was taken typical for the most DSMC applications, $Z_v = 50$. The temporal homogeneous relaxation of heated oxygen, $O_2$, is given in Fig. 2. Initially, $T_{\mathrm{trans}} = T_{\mathrm{rot}} = 20{,}000$ K, $T_{\mathrm{vib}} = 0$, and $n = 10^{19}/\mathrm{m}^3$. For the VVT model, the gas relaxes to equilibrium much slower than for the LB model. For both models, the temperatures of different modes coincide at equilibrium. This example clearly shows the difference in vibrational relaxation lengths between the quasiclassical and conventional LB models. The influence of this difference on axisymmetric flow will be examined in the next section.

### Hyperboloid with a Flare

The computations were performed for the flow about a hyperboloid with a flare. The main goal was to clarify an impact of vibrational relaxation on the flowfields and macroparameters under re-entry conditions. Hyperboloid has a Hermes-like shape, its flap was deflected at 33 deg, and the flap length was 30% of the hyperboloid length. The freestream conditions were $T_\infty = 189$ K, $U_\infty = 7500$ m/s, and $Kn = 0.003$.

First, to distinguish the influence of vibrational energy transfer, the computations were conducted for nonreacting oxygen. The vibrational temperature flowfields are presented in Fig. 3 for three models: the conventional LB model with constant $Z_v = 50$, the model with VT and without VV transitions (VT model), and the VVT model. The variable molecular diameters were used in the last two models. Comparison of Fig. 3a with Figs. 3b and 3c shows a considerable difference in the flowfields as a result of the difference in vibrational relaxation

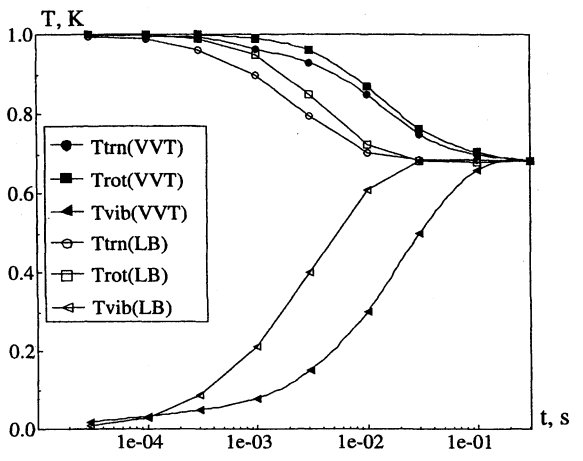


**Fig. 2 Temporal relaxation of different temperatures for LB and VVT models.**

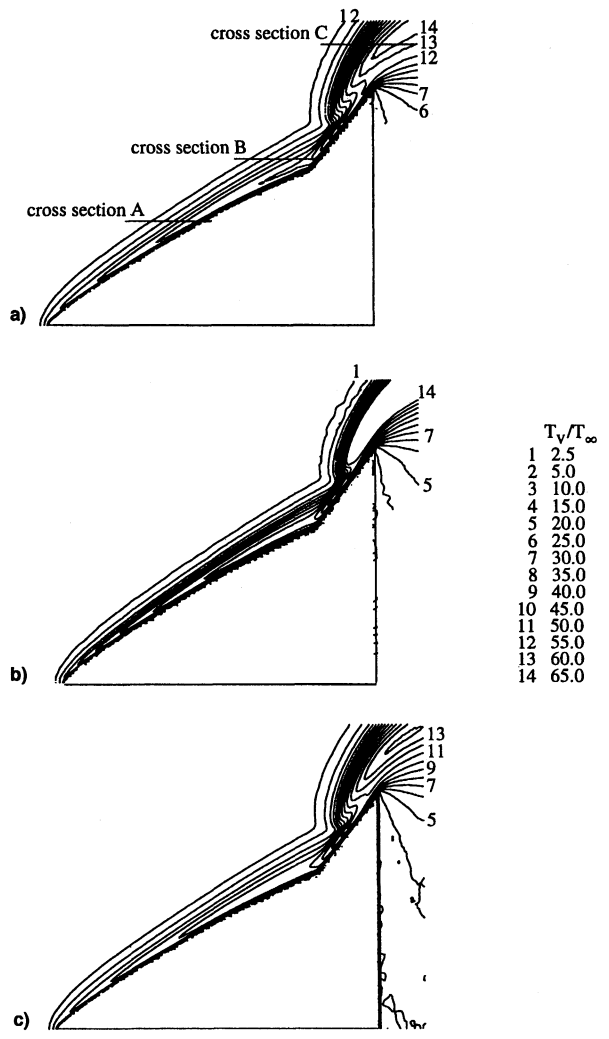


**Fig. 3 Influence of vibrational relaxation time and VV exchange on vibrational temperature: a) LB, b) VT, and c) VVT.**

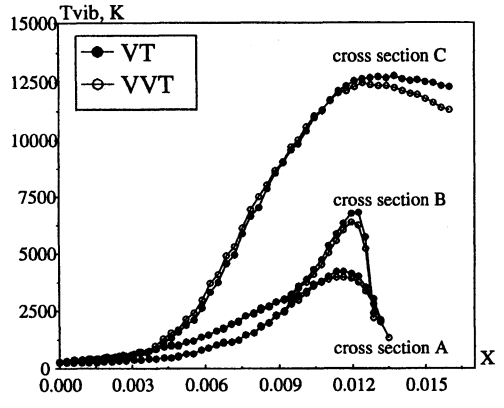


**Fig. 4 Vibrational temperature in different cross sections: impact of VV exchange.**

lengths. The results for VT and VVT models are not significantly different. These are compared in more detail in Fig. 4, where vibrational temperatures are given in different cross sections (the cross sections are plotted in Fig. 3b). It can be seen that VV energy transfer leads to the decrease of vibrational temperature. This is caused by the following reasons. Because the distance between energy levels decreases with the level number, in a case when the vibrational temperature is higher than the translational one, the vibrational quanta exchange leads to an increase of higher levels of population. This process is accompanied by the energy transfer from vibrational degrees of freedom to translation ones. As a result, the vibrational temperature is lower if the VV transitions are taken into account. It should be noted here that the influence of VV processes is higher in the domains where the difference between vibrational and translational temperatures is larger. This is the case along those cross sections where the rarefaction takes place. Comparison of other macroparameter profiles manifested an even smaller difference between VT and VVT models.

A strong thermal nonequilibrium is observed in the relaxation zone in front of a body. That is clearly seen in Fig. 5, where the temperatures of different mode are presented. The slow vibrational relaxation of the VVT model results in the large distance between the oblique shock and the surface. Besides the comparison of models with different vibrational relaxation times, this figure also illustrates the effect of variable molecular diameters [vibrational temperature for the VVT model with constant molecular diameters, $T_{\text{vib(c.d.)}}$, is presented]. It is clearly seen that the profiles for constant and variable diameters practically coincide. Other parameters are also very close for these two cases.

Computations were performed for dissociating $O_2$. Vibrational relaxation time significantly affects the degree of dissociation. Because the VVT model gives a vibrational temperature much less than the LB model, the degree of dissociation for this model is considerably smaller. The difference is particularly noticeable near the leading edge and slightly downstream. This is clearly seen in Fig. 6, where the atomic oxygen mole fractions in cross section A are presented. An interesting detail here is that the O concentration is larger in the case when VV exchange is taken into account (cf. VT and VVT models), despite the larger vibrational temperature for the VT model. This is connected with the previously men-

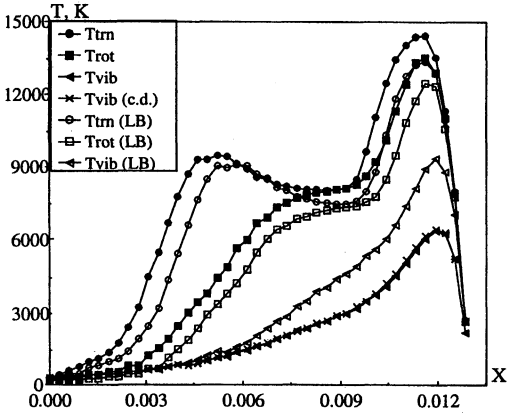


**Fig. 5 Effect of vibrational relaxation time and variable diameters on temperature profiles in cross section B.**

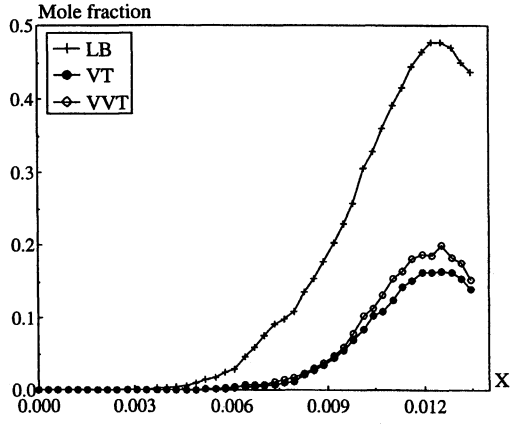


**Fig. 6 Atomic oxygen mole fractions for different models of reacting gas. Cross section A.**

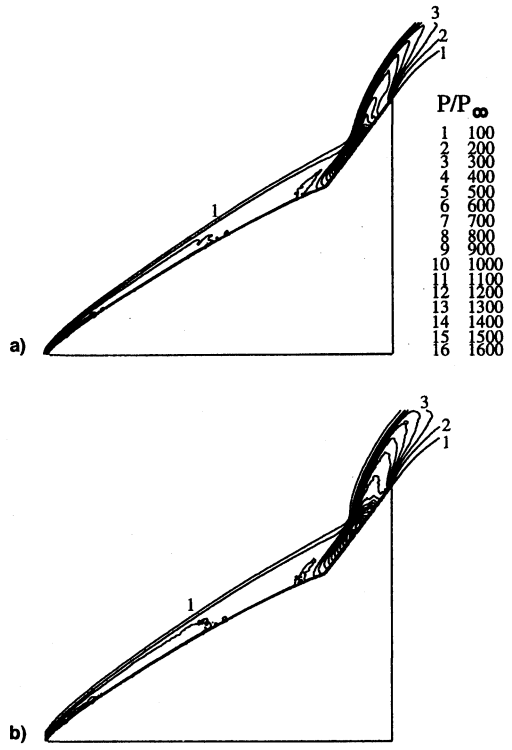


Fig. 7 Pressure fields: a) LB and b) VVT.

tioned effect of a larger population of higher levels that causes intensification of the dissociation process. Generally, the important conclusion from the comparisons of results for VT and VVT models is that at re-entry conditions the impact of VV transitions is visible but not determining.

The influence of different vibrational relaxation times for LB and VVT models of vibrations on the pressure flowfields is visible (Fig. 7); though it is not so large as for the mole fractions. The main difference is observed near the flap where it is smaller for the VVT model. This is also seen from the surface distribution of the pressure coefficient (Fig. 8a). The difference on the flap is also noticeable for the skin friction coefficient (Fig. 8b). For the heat transfer coefficient (Fig. 8c) the difference is also observed on the first half of the body. As the degree of dissociation is smaller for the VVT model, the heat transfer coefficient is less in this region.

### Flow About a Wedge

For $Kn \sim 10^{-3}$ and the temperature behind the shock of the order of 10,000 K, the relaxation zone for the vibrational mode is of order of the flow characteristic size. An impact of the vibrational model is the most pronounced in this case. There are very few experimental data available on the flows under such conditions. This is probably connected with the complexity of the simulation of high-enthalpy rarefied flows in ground facilities. The real gas effects were mainly examined for high-density flows ($Kn \sim 10^{-4}$–$10^{-5}$).

Near-continuum flows with $Kn \sim 10^{-4}$ have been investigated experimentally.[15] In this case the principal attention was paid to the study of relaxation effects on the standoff distance, $\Delta$, for a flow about a two-dimensional wedge placed symmetrically in a uniform supersonic flow. These results give an opportunity for a comparison with numerical data. The computations have been performed for the following flow conditions[15]: $U_\infty = 5500$ m/s, $T_\infty = 1100$ K, $\rho_\infty = 2.6 \times 10^{-3}$ kg/m$^3$, $T_w = 300$ K, and the freestream test gas consisted of 19.4% N and 80.6% $N_2$. The wedge length was $w = 0.051$ m. The stagnation temperature was 9070 K, which guarantees the excitation of vibrational degrees of freedom and nitrogen dissociation.

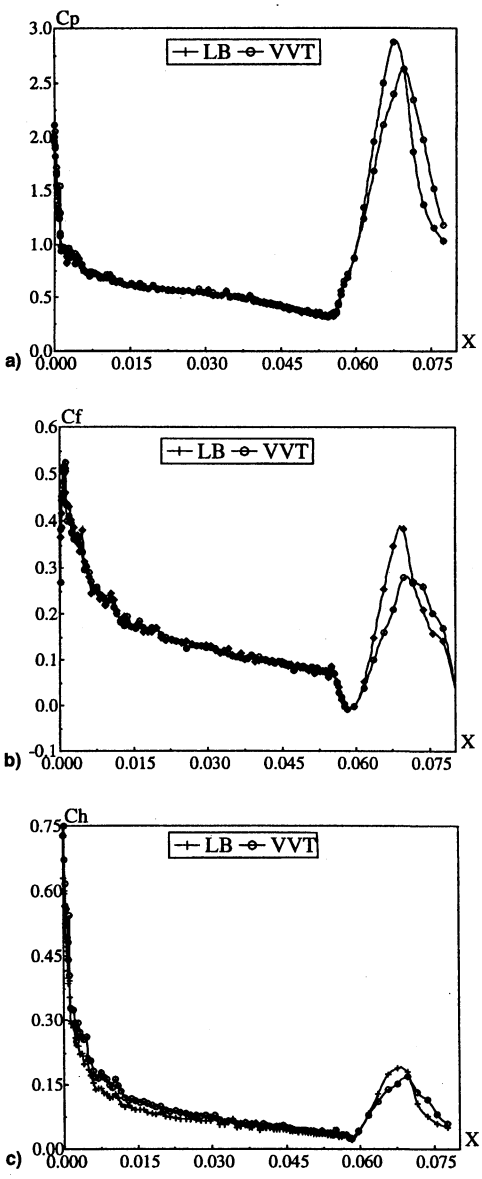


Fig. 8 Surface parameters for a hyperboloid with flare: a) pressure coefficient, b) skin friction coefficient, and c) heat transfer coefficient.

The DSMC computations, besides the standoff distance, enable one to obtain detailed information on the flowfields and flow nonequilibrium in the relaxation zone behind the shock wave. A typical pattern of a flow about a wedge is presented in Fig. 9 for the wedge angle $\delta = 51$ deg. The Mach number flowfield is presented here, obtained with the VVT model of dissociating nitrogen.

The profiles of mode temperatures in the cross section A are given in Fig. 10 for this case. The width of the thermal relaxation zone can be estimated as ~0.003 m. In addition to the large difference between temperatures in the shock front, a small difference is also observed in the boundary layer.

To assess the real gas effects, the computations were performed for a gas without vibrations and chemistry (TR gas) and reacting nitrogen (LB and VVT models). The dependence of the normalized standoff distance, $\Delta/w$, on $\delta$ is close to linear for TR gas (Fig. 11). The real gas effects (VVT model) make the standoff distance grow gradually as the wedge angle is increased. The difference between the two cases is considerable. All of this behavior agrees with the conclusions of Ref. 15. The computed values slightly underestimate the experimental data. The LB model gives an even smaller standoff distance than the VVT model.

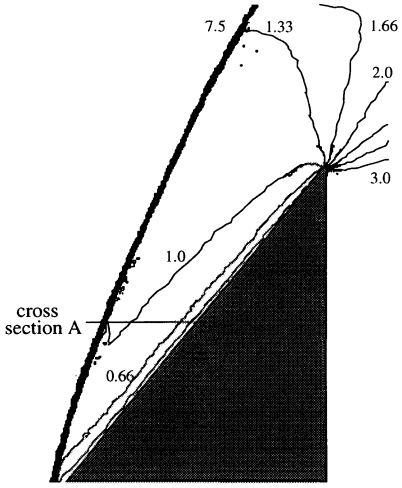


**Fig. 9 Mach number field over a wedge.**

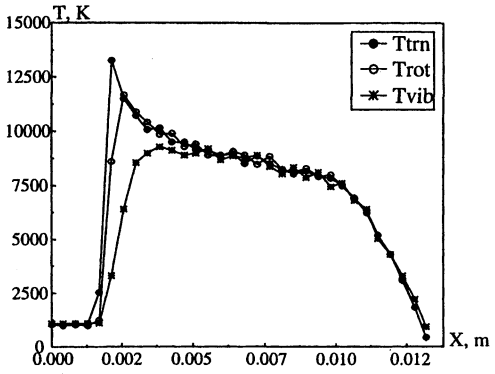


**Fig. 10 Mode temperatures in cross section A.**

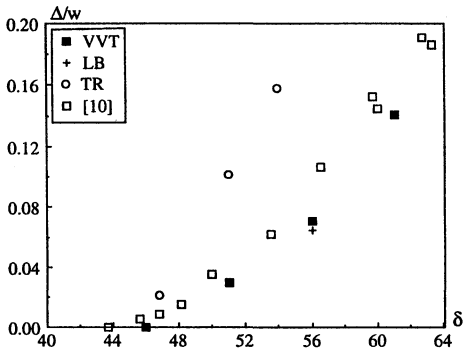


**Fig. 11 Standoff distance as a function of δ.**

## Conclusions

A new model was presented for the vibrational mode based on a quasiclassical approximation of the scattering theory. The VV energy transfer and the dependence of molecular diameters on rotational and vibrational states of a molecule were included. Calculations of homogeneous adiabatic relaxation showed a considerably smaller vibrational relaxation time for the present model as compared with the conventional LB model with constant $Z_v = 50$.

The difference in relaxation time was also found to be important for the flow about a hyperboloid with a flare at re-entry conditions. For this flow, the inclusion of VV energy transfer results in a small decrease of the vibrational temperature and at the same time in an increase of dissociation degree. The variation of molecular diameters depending on a rotational-vibrational state has no visible effect on the flowfields under the conditions considered here.

The comparison of computed and available experimental results with the standoff distance was presented for the dissociating nitrogen flow about a wedge. The computed standoff data slightly underestimates experimental data. The reasons for this difference will be in a future work.

## References

[1]Bogdanov, A. V., Dubrovskii, G. V., Gorbachev, Yu. E., Strelchenya, V. M., "Theory of Vibrational and Rotational Excitation of Polyatomic Molecules," *Physical Reports*, Vol. 181, No. 3, 1989, pp. 121–206.

[2]Gimelshein, S. F., Gorbachev, Yu. E., Ivanov, M. S., and Kashkovsky, A. V., "Real Gas Effects on the Aerodynamics of 2D Concave Bodies in the Transitional Regime," *Proceedings of the 19th International Symposium on Rarefied Gas Dynamics*, edited by J. Harvey and G. Lord, Vol. 1, Oxford Univ. Press, Oxford, England, UK, 1995, pp. 556–563.

[3]Ivanov, M. S., and Rogasinsky, S. V., "Theoretical Analysis of Traditional and Modern Schemes of the DSMC Method," *Proceedings of the 17th International Symposium on Rarefied Gas Dynamics* (Aachen, Germany), edited by A. E. Beylich, VCH, Weinheim, Germany, 1990, pp. 629–642.

[4]Ivanov, M. S., Antonov, S. G., Gimelshein, S. F., and Kashkovsky, A. V., "Computational Tools for Rarefied Aerodynamics," *Rarefied Gas Dynamics: Theory and Simulations. Proceedings of the 18th International Symposium on Rarefield Gas Dynamics*, edited by B. D. Shizgal and D. P. Weaver, Vol. 160, Progress in Astronautics and Aeronautics, AIAA, Washington, DC, 1994, pp. 115–126.

[5]Koura, K., and Matsumoto, H., "Variable Soft Sphere Molecular Model for Inverse-Power-Law of Lennard-Jones Potential," *Physics of Fluids A*, Vol. 3, No. 10, 1991, pp. 2459–2465.

[6]Bird, G. A., *Molecular Gas Dynamics and Direct Simulation of Gas Flows*, Oxford Univ. Press, Oxford, England, UK, 1994, pp. 208–217.

[7]Boyd, I. D., "Relaxation of Discrete Rotational Energy Distributions Using a Monte Carlo Method," *Physics of Fluids A*, Vol. 5, No. 9, 1993, pp. 2278–2286.

[8]Haas, B. L., Hash, D., Bird, G. A., Lumpkin, F. E., and Hassan, H., "Rates of Thermal Relaxation in Direct Simulation Monte Carlo Methods," *Physics of Fluids A*, Vol. 6, No. 6, 1994, pp. 2191–2201.

[9]Parker, J. G., "Rotational and Vibrational Relaxation in Diatomic Gases," *Physics of Fluids*, Vol. 2, No. 4, 1959, pp. 449–462.

[10]Bogdanov, A. V., Gorbachev, Yu. E., and Tiganov, I. I., "Analytical Approximations of Collision Cross-Sections and Collision Frequencies for Model Potentials," *Preprint of Physical–Technical Institute*, Physical–Technical Inst., Leningrad, No. 893, 1984.

[11]Gorbachev, Y. E., and Kunc, J. A., "Molecular Diameters of Rotationally and Vibrationally Excited Diatomic Molecules," *Physica A*, Vol. 247, Nos. 1–2, 1998, pp. 108–120.

[12]Gorbachev, Y. E., and Mallinger, F., "A Quasi-Classical Model for VT and VV Rate Constants," Rapport de Recherche d'Institut National de Recherche en Informatique et en Automatique (INRIA), INRIA Rocquencourt, Paris, France, No. 3331, Jan. 1998.

[13]Millikan, R. C., and White, D. R., "Systematics of Vibrational Relaxation," *Journal of Chemical Physics*, Vol. 39, No. 12, 1963, pp. 3209–3213.

[14]Losev, S. A., Makarov, V. N., Pogosbekyan, M. J., Shatalov, O. P., and Nikolsky, V. S., "Thermochemical Nonequilibrium Kinetic Models in Strong Shock Waves on Air," AIAA Paper 94-1990, June 1994.

[15]Hornung, H. G., and Smith, G. H., "The Influence of Relaxation on Shock Detachment," *Journal of Fluid Mechanics*, Vol. 93, Pt. 2, 1979, pp. 225–239.